Mg/Ca ratios in freshwater microbial carbonates: Thermodynamic , Kinetic and Vital Effects.

P. Saunders[a], M. Rogerson[a*], J.D. Wadhawan[b], G. Greenway[b], H.M. Pedley[a]

[a] Department of Geography, Environment and Earth Science, University of Hull, Cottingham Road, Hull, HU6 7RX, UK.

[b] Department of Chemistry, University of Hull, Cottingham Road, Hull, HU6 7RX, UK.

[*] Corresponding author: m.rogerson@hull.ac.uk

Abstract

The ratio of magnesium to calcium (Mg/Ca) in carbonate minerals in an abiotic setting is conventionally assumed to be predominantly controlled by $(Mg/Ca)_{solution}$ and a temperature dependant partition coefficient. This temperature dependence suggests that both marine (e.g. foraminiferal calcite and corals) and freshwater (e.g. speleothems and surface freshwater deposits, "tufas") carbonate deposits may be important archives of palaeotemperature data. However, there is considerable uncertainty in all these settings. In surface freshwater deposits this uncertainty is focussed on the influence of microbial biofilms. Biogenic or "vital" effects may arise from microbial metabolic activity and / or the presence of extracellular polymeric substances (EPS). This study addresses this key question for the first time, via a series of unique through-flow microcosm and agitated flask experiments where freshwater calcite was precipitated under controlled conditions. These experiments reveal there is no strong relationship between $(Mg/Ca)_{calcite}$ and temperature, so the assumption of thermodynamic fractionation is not viable. However, there is a pronounced influence on $(Mg/Ca)_{calcite}$ from precipitation rate, so that rapidly forming precipitates develop with very low magnesium content indicating kinetic control on fractionation. Calcite precipitation rate in these experiments (where the solution is only moderately supersaturated) is controlled by biofilm growth rate, but occurs even when light is excluded indicating that photosynthetic influences are not important. Our results thus suggest the apparent kinetic fractionation arises from the electrochemical activity of EPS molecules, and are therefore likely to occur wherever these molecules occur, including stromatolites, soil and lake carbonates and (via colloidal EPS) speleothems.

1. Introduction

The potential of the $(Mg/Ca)_{calcite}$ palaeothermometer was first observed in the 1950's when a link between latitude and magnesium content was recognised in a study on the

biogeochemistry of marine skeletal calcites (Chave, 1954). The use of $(Mg/Ca)_{calcite}$ ratios as a palaeothermometer has since become widespread in marine settings with many studies on benthic and planktonic foraminifera (Delaney *et al*., 1985, Nurnberg *et al*., 1996, Rosenthal *et al*., 1997, Anand *et al*., 2003, Elderfield *et al*., 2006, Kisakurek *et al*., 2008, Bousetta *et al*., 2011, Martinez-Boti *et al*., 2011) and to a lesser extent in corals (Mitsuguchi *et al*., 1996, Shirai *et al*., 2005, Wei *et al*., 2000; Yu *et al*., 2005, Reynaud *et al*., 2007). Surface freshwater carbonates ("tufa") are ambient temperature freshwater deposits which have been considered, but not thoroughly investigated, as potential archives of terrestrial palaeotemperature data through their Mg/Ca ratios (Garnett *et al*., 2004; Rogerson *et al*., 2008, Brasier *et al*., 2010, Lojen *et al*., 2009).

A number of divalent cations are able to substitute for the position of Ca^{2+} in the calcite crystal structure. The degree to which this substitution occurs is generally expressed through a partition coefficient (K_d). The heterogeneous partition coefficient for the partitioning of Mg^{2+} between a carbonate mineral and the aqueous solution is given by the equation (Oomori *et al*., 1987):

$$log\frac{\left(m_{Mg^{2+}}\right)_i}{\left(m_{Mg^{2+}}\right)_f} = \lambda_{Mg}\frac{(m_{Ca^{2+}})_i}{(m_{Ca^{2+}})_f}$$

Where m is the concentration of the subscripted species and i and f represent the initial and final solutions respectively. In the carbonate literature the partition coefficient is usually expressed in the general simple form:

$$K_d = \frac{\left(Tr/Ca_{CaCO_3}\right)}{(Tr/Ca)_{soln}}$$

Where Tr is the trace cation and K_d is the partition coefficient. Mg/Ca palaeothermometry therefore relies on the thermodynamic control of the partitioning of trace elements in the carbonate crystal lattice being sufficiently dominant from other effects so as to reduce them to "noise". Studies on inorganic calcite have confirmed that, under controlled conditions, the dominant control on Mg partitioning in carbonates is indeed temperature, with other factors such as precipitation rate having little influence (Mucci, 1987, Morse and Bender, 1990). However, evidence from natural (i.e. non-controlled) conditions shows the value of K_d to be dependent on significant complicating factors arising from precipitation rate, crystal

morphology and spatially / temporally variable solution composition (Fairchild and Treble, 2009).

1.1 Mg/Ca in Tufa carbonates and the conjectured role of Extracellular Polymeric Substances.

To date very few studies have had any real focus on utilising tufa $(Mg/Ca)_{calcite}$ ratios as a palaeothermometer. Incorporation of Mg^{2+} into tufas deposited in the summer was found to be higher than in winter (Chafetz *et al*., 1991) and a seasonal temperature change in stream water of ~ 10 °C appeared to be the dominating influence on Mg^{2+} incorporation into a 14 year (1985 – 1999) tufa record from Queensland Australia, although there were considerable discrepancies in the correlation between the tufa $(Mg/Ca)_{calcite}$ ratios and water temperature (Ihlenfeld *et al*., 2003). Although these studies show support for the potential of tufa $(Mg/Ca)_{calcite}$ palaeothermometry they do not take into account the presence of microbial biofilms and the significant impact they may have on trace element incorporation into tufa carbonates. The discrepancies observed by Ihlenfeld *et al.*, (2003) may be due to the presence of a spatially inconsistent and heterogeneous microbial biofilm with its associated metabolism and/or the chemoselective chelation of cations from the river water by EPS molecules.

Unlike corals and foraminifera, where all precipitation is biogenic (Elderfield *et al*., 1996, Yoshimura *et al*., 2011) and speleothems where precipitation is usually assumed to be abiogenic (although biogenic precipitation has been demonstrated, e.g. (Cacchio *et al*., 2004), the role of biology in determining tufa carbonate chemistry is poorly understood (Pedley et al., 2009). Recent research efforts have been focussed on the impact of the presence of extracellular polymeric substances (EPS), which have the capacity to be a first-order control on the precipitation chemistry (Dittrich *et al.*, 2003, Bissett *et al.*, 2008). EPS has demonstrated the ability to bind divalent cations, resulting from the fact that most EPS molecules have negatively charged functional groups which deprotonate as pH increases (Konhauser, 2007, Dittrich and Sibler, 2010). Studies on cyanobacteria and sulphate reducing bacteria (SRB) have revealed that the functional groups include carboxylic acids (R-COOH), hydroxyl groups (R-OH), amino groups ($R\text{-}NH_2$), sulphate ($R\text{-}O\text{-}SO_3H$), sulphonate ($R\text{-}SO_3H$), and sulphydryl groups (-SH), all of which bind metal ions including Ca^{2+} and Mg^{2+} (Dupraz *et al*., 2009 and references therein). It has been demonstrated that chelation strongly favour ions with low charge density thus favouring Ca^{2+} over Mg^{2+} (Rogerson *et al.*, 2008).

This influence could be transmitted to solid carbonate chemistry by altering the M^{2+} / Ca^{2+} ratios within the biofilm interstitial waters from which carbonates are precipitated and also by directly influencing the precipitation mechanism itself. Variations in trace element chemistry within hyper-alkaline lacustrine carbonate have recently been identified, with high calcium carbonates presented in close proximity to cells (Couradeau et al., 2013). However, the direct link to EPS intermediary states remains untested.

The primary mechanism by which EPS electroselectivity can be transmitted to precipitates arises from the fact that chelation of ions is not a permanent state, ions constantly move between bound states and solution. The ratio of ions in the solution in the immediate vicinity of the chelation sites is consequently determined by the binding preferences of the EPS. As Ca^{2+} is selectively favoured over Mg^{2+} by EPS molecules then the $(Mg/Ca)_{solution}$ in this environment will be reduced relative to the bulk water. Therefore, calcite precipitation initiated on a calcite surface covered in biofilm will occur at the nucleation sites enriched with calcium ions relative to magnesium. Any precipitates forming in the immediate environment of the EPS will therefore have a $(Mg/Ca)_{calcite}$ lower than would be expected given the bulk water $(Mg/Ca)_{solution}$.

The generation of low $(Mg/Ca)_{calcite}$ within the EPS matrix will be accentuated by the low Mg^{2+} concentrations in this microenvironment. It has been demonstrated that calcite precipitation rates are reduced in the presence of Mg^{2+} (Morse and Mackenzie, 1990, Paquette *et al*., 1996, Zhang and Dawe, 2000) and that this reduction is approximately proportional to the $(Mg/Ca)_{solution}$ (Morse and Mackenzie, 1990, Zhang and Dawe, 2000). Therefore the lower $(Mg/Ca)_{solution}$ in the immediate microenvironment of the EPS molecules created by the chemoselectivity for Ca^{2+} will result in a faster precipitation rate in these regions of the biofilm compared to other areas where the $(Mg/Ca)_{solution}$ is greater. This effect will become cumulative at higher precipitation rates, driving down the mean $(Mg/Ca)_{calcite}$ of precipitates generated within the biofilm.

This study tests the hypothesis that the presence of biofilm results in precipitation of reduced $Mg/Ca_{(calcite)}$ for the first time, and also tests whether this effect is sufficient to suppress classic thermodynamic controls for the first time.

2. Methods

2.1 Experimental design

The microcosm system was based on the recirculating flume system developed at the University of Hull (Rogerson et al., 2010, Pedley et al., 2009). It was designed to allow the flow through of experimental water through a series of four identical micro-flumes. The design is shown in Figure 1 (which also includes the experimental design of the additional conical flask experiments (see section 2.4)). The apparatus was housed in a windowless, air conditioned laboratory where the ambient laboratory air temperature was maintained between 16 and 20 °C by an 'Airforce Climate Control' air conditioning unit (10,000 BTU hr^{-1}; 2.9 kW cooling capacity, Airconwarehouse, Stockport, UK). This provided the experiments some buffering from variations in room temperatures due to seasonal and diurnal changes. Experiments were performed for a period of 28 days and consisted of four replicates which were run within identical Perspex micro-flumes with dimensions of 20 cm by 8 cm and a depth of 2.5 cm. Each flume was constructed with a 7 mm wide flow channel with a Perspex lid providing a water tight seal. For the duration of the experimental runs the flumes were submerged in a metallic water bath to ensure tight control on precipitation temperature. Experiments were conducted at 12 ± 0.2, 14 ± 0.2, 16 ± 0.2, 18 ± 0.2 and 20 ± 0.5 °C (Saunders *et al*., in press).

The water bath temperature was controlled via a Titan 150 mini cooler chiller unit (Aqua Medic, Bisendorf, Germany).Water was re-circulated through the chiller unit via a submerged pump in the sump and the bath itself was surrounded by sheets of thermal aluminium foil (thermal resistance 1.455 m^2 K W^{-1}) to provide additional thermal buffering and exclude incoming UV from the water bath. Only the micro-flumes were left exposed to the lighting unit to allow photosynthesis. Sheets of thermal aluminium foil were placed over piping which was external to the water bath to prevent heating from the lighting unit. The chiller unit was able to provide temperature control at 12, 14, 16 and 18 °C. The unit was unable to maintain the water temperature at 20 °C so additional heating was provided by a thermostatically controlled Aqua One 100 W fully submersible aquarium heater (Aqua Pacific Ltd., Southampton, UK) placed in the sump. The temperature of the water bath was monitored at ten minute intervals via a calibrated thermometer probe (range -50 to 200 °C) (Thermometers Direct, Aldershot, UK) inserted next to the microcosms. The digital output from the thermometer was recorded to a PC via a webcam system, so each experiment is represented

by over 4000 individual recorded water temperature measurements. Photosynthetic light was supplied to the system via a single 'Thorn Lopak 250 W HPS-T' sodium lamp on a 7 hour on and 17 hour off cycle to avoid excessive light incidence, which previous experiments had demonstrated bleached the biofilm.

2.2 Biofilm

Biofilm was sourced from the River Lathkill, Derbyshire (UK grid reference SK 225 645). Initial colonisation was onto carbon fabric secured to house bricks which were submerged in an active tufa precipitating reach on the 3rd of April 2009 and recovered on the 5th of August 2009. To ensure a constant supply of a common biofilm, which was free of "inheritance" calcite, the colonised carbon fabric was detached from the bricks and secured within a 1 metre long, 112 mm wide polycarbonate gutter within a mesocosm (see Rogerson et al., 2009 and Pedley et al., 2009). 30 L of deionised (15 MΩ) water was circulated between the colonising gutter and a sump via a Titan 150 in line chiller set at 12 °C. The colonising flume was illuminated by a single 'Thorn Lopak 250 W HPS-T' hydroponic lamp on a 7 hour on and 17 hour off cycle. This "colonisation" flume was used to colonise clean plastic mesh pads, after which the source biofilm was removed and the water replaced with fresh, 15 MΩ water. The colonisation process was continued for a further 3 months to achieve a sustainable amount of completely sediment-free and carbonate-free biofilm for all future experiments. To avoid nutritional deprivation a 30 ml dose of an organic liquid was added at monthly intervals. The organic liquid was obtained from the decomposition of tree leaves from Welton Beck catchment (water source for the colonising flume). This nutritional regime had proved successful in previous experiments within the same laboratory (see Pedley *et al*., 2009), and minimises the change in the balance of diatoms and cyanobacteria inevitable once a biofilm body is removed from its natural environment.

Prior to the first experiment a sample of the newly colonised biofilm was taken and prepared for examination by scanning electron microscopy (SEM). No calcite precipitates could be observed, and the culture visually resembled the source biofilm in terms of its biological composition.. Ecologically, the biofilms comprised a mixed diatom and cyanobacterial mat associated with a variety of bacterial taxa not possible to identify visually. EPS found in cultured films were similar in appearance and density as those found in the field. Experimental biofilm was recovered via standard glass microscope slides cut to 5 mm wide

strips and frosted with corundum glass frosting powder which were secured to the colonised mesh pads and could be removed and imported into the micro-flumes immediately and without further alteration.

2.1 Trace element analysis

All water chemistry analyses was undertaken on a Perkin Elmer Optima 5300DV (Perkins-Elmer, Waltham, MA, USA) inductively coupled optical emission spectrometer (ICP – OES). The selection of the analytical lines used in the results was based on the Perkin Elmer recommendations for the Optima 5300 DV spectrometer, 393.366 nm for calcium and 280.271 nm for magnesium. Calibration standards were prepared using 1000 ppm standard stock solutions (99.9% pure or greater, PrimAg, Xtra, Romil, Cambridge) of calcium and magnesium. Mixed standards of calcium and magnesium were prepared through dilution with 2% ultrapure HNO3 to give calibration standards of 1, 2, 3, 4 and 5 ppm for calcium and 0.1, 0.2, 0.3, 0.4, and 0.5 ppm for magnesium. Samples for analysis were diluted with 5 % ultrapure HNO_3 to bring the expected concentrations to within or very near the linear calibration of the standards.

2.2 Experimental solution

Initial water for the experiments was collected from a spring sourced by a Cretaceous chalk aquifer at Welton Beck, East Yorkshire (UK grid reference SE 965 275). Although there were variations in springwater chemistry, the concentrations of $Mg^{2+}_{(aq)}$ and $Ca^{2+}_{(aq)}$ in the spring water were fairly stable ranging from 2.6 – 5.1 mg L^{-1} for magnesium and 82.9 – 141.2 mg L^{-1} for calcium. To ensure the water for all experiments had equal levels of $Mg^{2+}_{(aq)}$ and $Ca^{2+}_{(aq)}$ acetates of calcium ($Ca(C_2H_3O_2)_2$ and magnesium ($Mg(C_2H_3O_2)_2$ (Alfa Aesar, Massachusetts., USA) were added to the spring water to bring the concentrations of $Mg^{2+}_{(aq)}$ and $Ca^{2+}_{(aq)}$ to 8.0 and 160 mg L^{-1} respectively giving a constant $(Mg/Ca)_{solution}$ molar ratio of 0.082. The pH of the source water was rather invariable at 8.2 ±0.2, and bicarbonate alkalinity 180 ± 22 mg L^{-1}. The solution was analysed before and after addition to ensure minimum variance in this composition, and therefore changes in solution chemistry throughout the experiments described herein are negligable. Acetates were used to avoid contaminating the solution with variable levels of exotic counter-ions; organic acids were already present in high concentrations in the dissolved components of the EPS and considered the most “inoffensive” counter ion in our context. The saturation state was

determined using the aqueous geochemical modelling software PHREEQC. Saturation index values for the experimental solutions were 0.95, 0.98, 1.01, 1.04 and 1.07 for the temperatures, 12, 14, 16, 18 and 20 °C respectively

2.3 Precipitate recovery

At the end of each experiment the glass slides containing the biofilm and experimental precipitates were removed from the microcosms and the biofilm covering of the glass slide was added to 20 mL sterilin tubes and centrifuged in a Centaur 2 non refrigerated bench top centrifuge (MSE, London, UK) at 3300 rpm for 20 minutes. The supernatant water was discarded. Prior to dissolution of the calcite precipitates in the biofilm it was necessary to 'clean' the biofilm of Mg^{2+} and Ca^{2+} cations that had been chelated by the EPS of the biofilm complex. Ultrapure water (18 MΩ) was added to each tube containing the biofilm pellet. The tube was shaken vigorously to ensure full mixing of the biofilm with the water and left to stand for two hours. It was then centrifuged at 3500 rpm for 15 minutes. A sample was taken of the supernatant and immediately acidified with 5 % ultrapure HNO_3 for analysis of the $Mg^{2+}_{(aq)}$ and $Ca^{2+}_{(aq)}$ levels by ICP – OES. This process was repeated five or six times to ensure all practical chelated Mg^{2+} and Ca^{2+} cations were washed from the biofilm (as confirmed by ICP – OES analyses). The biofilm pellet was then oven dried. The dissolution of calcite precipitates held within the dried biofilm pellet was achieved by gravimetrically adding 10% ultrapure HNO_3 to the sample. The samples were sonicated for three minutes in an Ultra 8000 bench top ultrasonic cleaner (Ultrawave, Cardiff, UK) left to stand for two hours, shaken vigorously, sonicated again and centrifuged for 15 minutes at 3300 rpm. A sample of the supernatant was taken and immediately acidified with ultrapure 5 % HNO_3 for analysis of $Mg^{2+}_{(aq)}$ and $Ca^{2+}_{(aq)}$ levels and determination of the precipitate $(Mg/Ca)_{calcite}$ ratios.

2.4 Additional experiments

Additional experiments were conducted in 150 ml conical flasks. Experiments were conducted at 12 ± 0.5, 14 ± 0.2, 16 ± 0.3, 18 ± 0.2 and 20 ± 0.5 °C. The flasks were secured to a Stuart SF1 flask shaker (Bibby Scientific Limited, Staffordshire, UK) which was set to 100 oscillations per minute for all experiments to promote oxygenation of the solutions.

Eight 150 mL conical flasks were used with two replicates each of three different treatments and two controls. The treatments consisted of biofilm exposed to solar spectrum light (BFL)

and biofilm with light excluded (BFD). The biofilm used was taken from the same colonising flume as the microcosm experiments. Each flask for the biofilm treatments received 3 g of biofilm and 50 mL of prepared solution. The two flasks from which light was excluded were thoroughly wrapped in reflective thermal aluminium foil (thermal resistance 1.455 m^2 K W^{-1}) to exclude all light. Foam bungs were used to prevent microbial invasion and reduce evaporative loss from the flasks whilst allowing gas exchange. The flasks were clamped to the shaker and further thermal aluminium foil (thermal resistance 1.455 m^2 K W^{-1}) was used to cover the sections of the water tank containing the light excluded replicates. Solution preparation, the removal of chelated cations and precipitate recovery followed the procedures described for the microcosm experiments.

3. Results

3.1 $(Mg/Ca)_{calcite}$ and precipitation temperature

Binary plots of $(Mg/Ca)_{calcite}$ ratios and temperature for the microcosm and agitated flask experiments are shown in Figure 2. In all cases, control data (where precipitation is solely physical) shows a positive correlation to temperature, approximately conforming to the expected exponential correlation with $Mg/Ca = 0.0029e^{0.1568T}$ ($R^2 = 0.90$, $P < 0.05$). However, the microcosm data (Fig 2 (a)) does not conform to the expected relationship, instead it reveals a weak negative linear correlation between Mg/Ca and temperature in the presence of biofilm ($P < 0.05$, $R^2 = 0.44$) so that $(Mg/Ca)_{calcite}$ generally decreases as temperature increases. Apart from the 20 °C experiment there is considerable variation of $(Mg/Ca)_{calcite}$ ratios at a given temperature; at 14 °C there is nearly an order of magnitude range. The flask experiment data for both BFL and BFD follow an almost identical pattern to that of the microcosm data (Fig. 2 (b & c)), although again with considerable scatter. Two replicates have plots well off the general pattern; both are at 18 °C, one from the BFL and one from the BFD. The presence of the potentially anomalous data points at 18 °C results in no significant correlation between temperature and $(Mg/Ca)_{calcite}$ for the BFL or BFD experiments ($R^2 = 0.13$, and $R^2 = 0.16$ respectively). The exclusion of the anomalous data points results in a significant negative power relationship at the 95 % confidence level for both BFL ($R^2 = 0.76$) and BFD experiments ($R^2 = 0.88$) respectively. Combining the data generated from the microcosm and agitated flask experiments (Fig. 2 (d) gives no correlation between $(Mg/Ca)_{calcite}$ and temperature for precipitates generated in the presence of biofilm.

3.2 Temperature and precipitation rate

Binary plots of precipitation rates and temperature are presented in Figure 3. The microcosm data (Fig 3 (a)) present a significant ($P < 0.05$) exponential correlation ($R^2 = 0.86$). No significant correlation was found between precipitation rate and temperature for BFL precipitates (Fig 3 (b)) as data at 18 °C do not follow the general trend of increasing rate at higher temperatures observed at the other temperatures (excluding these points reveals a linear correlation; $P < 0.05$, $R^2 = 0.70$). The BFD precipitates (Fig. 3 (c)) reveal a linear correlation significant at the 95 % confidence level ($R^2 = 0.48$). The strength of this correlation is again reduced by the apparently anomalous data point at 18 °C, and removing this data point again strengthens the correlation ($R^2 = 0.74$). Combining the data from the microcosm and agitated flask experiments (Fig 3 (d)) results in an exponential relationship between precipitation rate and temperature ($P < 0.05$, $R^2 = 0.45$).

3.3 $(Mg/Ca)_{calcite}$ and precipitation rate

Figure 4 shows the relationship between $(Mg/Ca)_{calcite}$ and precipitation rate. The control data shows a significant linear correlation whereby $(Mg/Ca)_{calcite}$ increases as precipitation rates rise, which is consistent with theoretical expectations which predict that Mg^{2+} partitioning increases with increasing precipitation rate (Rimstidt *et al*., 1998). In complete contrast, the results from the microcosm experiments (Fig. 4 (a)) show a negative power correlation between the parameters ($R^2 = 0.52$, $P < 0.05$) with $(Mg/Ca)_{calcite}$ falling as precipitation rates increases. Similarly, the relationship between the $(Mg/Ca)_{calcite}$ ratios and precipitation rate for the BFL and BFD experiments (Fig. 4 (b & c)) takes the form of a negative power regression ($R^2 = 0.89$ and 0.83 respectively), and for both sets of data combined ($R^2 = 0.79$) all of which are significant at the 95 % confidence level. Figure 4 (d) plots the data from the microcosm, BFL and BFD experiments, the negative power correlation observed individually in the experiments is still held ($P < 0.05$, $R^2 = 0.67$), although there is a clear separation of the 20 °C data.

4. Discussion

4.1 Precipitation temperature and $(Mg/Ca)_{calcite}$

The experimental results reveal that the presence of a microbial biofilm overrides the expected thermodynamic control on $(Mg/Ca)_{calcite}$ in a freshwater environment, and that use

of tufa derived $(Mg/Ca)_{calcite}$ as a palaeothermometer would be ill-advised. The data is not random however, and the structure of relationships between the parameters clearly indicates some form of significant microbial control. However, the coherent response of experiments in the microcosms and flasks both in light and dark indicates that some other (non-thermodynamic) controls are in operation. Other than at 20°C, the microcosm data show wide variations in the $(Mg/Ca)_{calcite}$ indicating that these controls are not simple. The agitated flask experiments generally present a tighter relationship between $(Mg/Ca)_{calcite}$ and temperature, with the exception of two of the data points at 18 °C in both the BFL and BFD treatments. Examination of all the original ICP – OES outputs do not reveal anything that may make these values obviously erroneous, furthermore it cannot arise from some unexpected ecological change as the systems are fundamentally dissimilar one being largely heterotrophic and the other photosynthetic. The only common factor is that these flasks were seeded with the same aliquot of biofilm, and it is possible that this aliquot had a significantly different microbial or EPS composition which altered the behaviour of the biofilm in terms of calcite precipitation.

4.2 Temperature and calcite precipitation rate

At a given saturation state, calcite precipitation should increase with increasing temperature due to calcite solubility decreasing with increasing temperature (Morse and Mackenzie, 1990). Higher temperatures also increase precipitation rates through the increased kinetic energy of the species, a higher number of collisions between ionic species at higher energies will increase the likelihood of precipitation reactions overcoming the activation energy barrier and going to completion. Increased calcification rates at higher temperatures have been observed in laboratory experiments involving precipitation in the presence of bacterial isolates (Cacchio *et al*., 2003, Cacchio *et al*., 2004, Baskar *et al*., 2006), however, no studies appear to have been conducted which examine precipitation rates as a function of temperature in the presence of a full microbial biofilm.

We find no consistent relationship between the mean precipitation rates at a given temperature (Table 1) and the precipitation environment (e.g. the flow-through microcosms or the agitated flasks), but also no consistent differences between the three types of system (microcosm, BFL and BFD). At the commencement of the experiments the Ω values were the same for both microcosm and agitated flask experiments, and only marginally different within the entire range of conditions (Ω = 0.95 to 1.07), although in the agitated flasks there

was no replenishment of ions to the experimental solution so Ω values will have fallen over time as precipitation took place. In the absence of other reasons to explain the breakdown of the expected physicochemical behaviour, we again conclude that $Mg/Ca_{calcite}$ is controlled by microbial activity or the presence of EPS.

4.3 $(Mg/Ca)_{calcite}$ and precipitation rate

The negative power relationship between $(Mg/Ca)_{calcite}$ and precipitation rate derived from the microcosm and agitated flask experiments is contradictory to theoretical expectations suggesting that the presence of the biofilm has a strong influence on the correlation between the parameters. Distribution coefficients (*K*) were calculated for both microcosm and agitated flask precipitates using the standard equation $K = (Mg/Ca)_{calcite}/(Mg/Ca)_{solution}$ and are presented as a function of precipitation rate in Figure 5 ($P < 0.05$, $R^2 = 0.67$). However, empirical distribution coefficients differ from theoretical coefficients which are determined from a system assumed to be at equilibrium. Experimental conditions can only approximate equilibrium, furthermore kinetic effects result in non uniform trace element partitioning in precipitates from actual experiments (Rimstidt *et al*., 1998). For the purposes of the following discussion empirical coefficients will be designated by (K_{em}) and equilibrium coefficients by (K_{eq}). Table 2 shows the K_{em} K_{eq} and ionic radii for selected divalent cations. Experimental evidence shows that a relationship exists between precipitation rates and K_{em} which is dependent on the value of K_{eq} (Rimstidt *et al*., 1998) where:

for elements with a $K_{eq} < 1$ (e.g. Mg^{2+}) the value of K_{em} is larger than K_{eq} and decreases towards K_{eq} as precipitation rates fall.

for elements with $K_{eq} > 1$ the value of K_{em} is smaller than K_{eq} and increases towards K_{eq} as precipitation rates fall.

These relationships have been observed experimentally (e.g. Lorens, 1981, Mucci 1987, Pingitore *et al*., 1988, Tesoriero and Pankow, 1996) in abiotic precipitates. Accordingly, at faster precipitation rates the value of K_{em} for Mg^{2+} into calcite should increase as precipitation rates rise. The K_{em} values obtained in the experiments described here are in complete contrast to this and also to the K_{em} values obtained in experiments on inorganic calcite. Clearly, normal chemical evolution of the solid from the solution is being prevented by the biofilm.

4.4 The potential of biofilms to influence calcite precipitation chemistry

373 The presence of a microbial biofilm in these experiments has shifted the $(Mg/Ca)_{calcite}$ ratios
374 as a function of both temperature and precipitation rate away from theoretical expectations
375 but also from the type of relationships seen in other biogenic carbonates such as ostrocodes,
376 foraminiferal and coral carbonate. This indicates that trace element ratios and precipitation
377 rates must be influenced by some aspect of the biofilm not present in other settings; these
378 must be specific microbial metabolic processes, structural components of the biofilm (EPS)
379 or a combination of both. Temperature variations have been shown to have an impact on
380 both biofilm microbial diversity and growth rates from photosynthesis and heterotrophic
381 metabolism within the temperature range of the experiments described here (Blanchard *et al*.,
382 1996, Watermann *et al*., 1999, Defew *et al*., 2004, Hancke and Glud, 2004, Salleh and
383 McMinn, 2011). The diversity of microorganisms held in a laboratory grown biofilm exposed
384 to specific light and temperature conditions is strongly dependant on species specific growth
385 rates and any species within the biofilm complex can only acclimatise to the imposed
386 environment within their individual genetic limits (Defew *et al*., 2004). In
387 diatom/cyanobacterial biofilms such as those used in this work it has been observed that at 10
388 °C diatoms are the dominant organism but at 25 °C filamentous cyanobacteria dominate
389 (Watermann *et al*., 1999). Others have observed that between 10 and 18 °C changes in
390 diatom species composition were minimal, but at 18 °C there was a significant change in the
391 species composition, with a significant shift to low diversity (Defew *et al*., 2004). In light of
392 these observations it is assumed that over the range of 12 – 20 °C of the described
393 experiments considerable variation will have been induced in both genus and species
394 variations during the course of each experimental run.

395 Such changes in ecological structure will likely result in the changes in biogeochemical
396 behaviour found during our experiments. The finding of Waterman *et al*., (1999) that
397 cyanobacteria are the dominant organisms in biofilms at higher temperatures may explain the
398 dramatic increase in precipitation rates at 20 °C seen in the microcosm experiments. Biofilm
399 microprofiles of pH, O_2, Ca^{2+} and CO_3^{2-} obtained by Shiraishi *et al*. (2008) showed that bright
400 green cyanobacteria dominated biofilms had a higher photosynthetic capacity and thus
401 exerted more influence on the carbonate system at the tufa surface. The enhanced creation of
402 an alkaline environment through the greater photosynthetic capacity of a cyanobacterial
403 dominated biofilm at 20 °C in the experiments described here may have enhanced
404 precipitation rates significantly over those at the lower temperatures where cyanobacteria
405 were not the dominant microorganism.

However, faster precipitation arising from ecological changes effect provides no mechanism to provide the trend reversal in the Kr_{em} compared to the Kr_{eq}; this requires first-order alteration of the cationic biogeochemical system.

4.4.1 Impact of EPS on $(Mg/Ca)_{calcite}$

Involvement of a metal-organic phase at precipitation sites, which are actively exchanging ions with ambient water (Rogerson et al, 2010), does provide a means of altering apparent partition coefficients. The wide variations in $(Mg/Ca)_{calcite}$ ratios seen in the precipitates generated within the biofilms of the microcosm experiments thus are likely to be a consequence of heterogeneity in the composition of the functional groups within the biofilm matrix.

Variations in species diversity have been shown to have a large impact on the composition and amount of EPS produced (Di Pippo *et al*., 2009), this is important given its ability to chelate $Ca^{2+}_{(aq)}$ and $Mg^{2+}_{(aq)}$ from the bulk water of a calcite precipitating experimental solution or natural system (Rogerson et al., 2008). The chelating ability of EPS molecules depends on the availability of binding sites on negatively charged functional groups, which may be reduced by interactions between EPS molecules by causing them to become sterically inhibited or blocked (Dupraz *et al*., 2009). The nature of these interactions will vary alongside changes in biofilm composition. It has been suggested that the physical state of EPS also influences the binding abilities, whereby EPS in a gel state may bind more strongly with a particular cation than one in a loose slime state (Decho, 2000).

In addition to changes in binding abilities (i.e. the amount of a specific cation) there is a further potential influence on $(Mg/Ca)_{calcite}$ arising from EPS through chemoselectivity, especially as pervasive EPS has been found associated with carbonate precipitates down to the nm scale (Benzerara et al., 2006). The favouring for the chelation of $Ca^{2+}_{(aq)}$ over $Mg^{2+}_{(aq)}$ will ensure that water in the immediate microenvironment of the EPS will have a lower $(Mg/Ca)_{solution}$ than that of the bulk water and the water held within the biofilm matrix which is not in the immediate microenvironment of the EPS molecules. Although it has been shown that chelation exhibits an overall selectivity across a full biofilm based on charge density (Rogerson *et al*., 2008) it has also been demonstrated that some anionic groups differ in their chelation affinities for Ca^{2+} and Mg^{2+} with some favouring calcium over magnesium and vice versa (Table 3) (Wang *et al*., 2009).

The complexity of these interactions would suggest that these influences would be rather unpredictable and "noisy", but we find a rather well organised relationship between precipitation rate and $Mg/Ca_{(calcite)}$. We propose that the very high calcium contents exhibited at high precipitation rate is most likely to arise from utilisation of the metal pool chelated to the EPS molecules (dominated by Ca^{2+} due to chemoselectivity). The bound cations may form either unidentate or bidentate bonds with anionic functional groups on the EPS molecules. Bidentate bonds form when both positive charges on the $Ca^{2+}_{(aq)}$ are linked to anionic groups, forming bidentate bridges between EPS molecules (Geesey and Yang, 1989). Such an arrangement would be an inhibiting factor to calcite precipitation as free Ca^{2+} ions have been removed from solution reducing the saturation index with respect to calcite (Kawaguchi and Decho, 2002). However, if only one of the positive charges on a $Ca^{2+}_{(aq)}$ cation is complexed with an anion (unidentate bonding) it leaves the other positive charge free to bind with a CO_3^{2-} ion and initiate $CaCO_3$ precipitation by providing a nucleation site for further precipitation (Shiraishi *et al*., 2008, Decho, 2010). A further mechanism by which $Mg/Ca_{(calcite)}$ ratios may be reduced from expectation is through the incorporation unidentate Ca^{2+} - ligand complexes into the precipitating solid. Figure 6 provides a schematic illustration of unidentate/bidentate bonding and how nucleation sites may develop on the free positive charge of a unidentate bonded Ca^{2+}.

5 Conclusion

The experimental results indicate that microbial metabolism and/or the presence of EPS molecules overrides the expected thermodynamic control on $Mg/Ca_{(calcite)}$ in ambient temperature freshwater carbonate deposits. This was observed in both the flow through microcosm and agitated flask precipitates. A significant relationship was found between $(Mg/Ca)_{calcite}$ ratios and precipitation rate for both the microcosm and agitated flask experiments.

It has previously been reported that EPS preferentially chelates Ca^{2+} over Mg^{2+} resulting in the microenvironment around the EPS molecules being enriched in calcium over magnesium generating low $(Mg/Ca)_{calcite}$ compared to that expected from the bulk water $(Mg/Ca)_{solution}$ ratio (Rogerson et al., 2008). This chemoselectivity favours the formation of Ca^{2+} - ligand complexes, and the incorporation of some of these complexes into the precipitating solid will both decrease precipitation activation energy (via "gel templating") (Decho, 2010) and drive the $(Mg/Ca)_{calcite}$ ratio down from that expected from the bulk water $(Mg/Ca)_{solution}$ ratio at a

given temperature. Our data implies that this process is fundamental in controlling the trace element geochemistry of tufa carbonate.

Although several calibrations of the Mg/Ca palaeothermometer have been constructed for foraminiferal and coralline calcite the findings here strongly suggest that the calibration of a palaeothermometer is not a realistic prospect for tufa carbonates precipitated in the presence of microbial biofilms. The finding that metal inclusion into precipitated calcite is accentuated at low precipitation rates, and that the specific bonding character of cations and EPS molecules are the primary regulator of this relationship, has impact well beyond palaeothermometry. Generally, geoengineering practices where pollutants are extracted from solution into carbonates aim at acceleration of the precipitation process. Our finding is that this may always not be appropriate.

6. Acknowledgements

This research was supported by a University of Hull 80th Anniversary PhD scholarship. Mark Anderson and Mike Dennett are thanked for their technical assistance and for assisting in the running of the experiments. Tony Sinclair and Bob Knight are thanked for their assistance in running the SEM and ICP – OES instruments respectively.

7. References

Anand, P., Elderfield, H., Conte, M.H. (2003) Calibration of Mg/Ca thermometry in planktonic foraminifera from sediment trap time series. *Paleoceanography,* **18 (2)**, 1050.

Beer, T. (1996) *Environmental Oceanography*. CRC Press, Florida.

Benzerara, K., Menguy, N., Lopez-Garcia, P., Yoon, T.-H., Kazmierczak, J., Tyliszczak, T., Guyot, F. & Brown, G. E., Jr. 2006. Nanoscale detection of organic signatures in carbonate microbialites. *Proceedings of the National Academy of Sciences* **103**, 9440-9445.

Bhaskar PV, Bhosle NB (2006) Bacterial extracellular polymeric substance (EPS): a carrier of heavy metals in the marine food chain. *Environment Inernational*, **32**, 191–198.

Bissett, A., Reimer, A., de Beer, D., Shiraishi, F. and Arp, G., (2008) Metabolic microenvironmental control by photosynthetic biofilms under changing macroenvironmental temperature and pH conditions. *Applied Environmental Microbiol*ogy, **74(20),** 6306-6312.

Blanchard, G.F, Guarini, J.M, Richard, P., Gros, P., Mornet, F. (1996) Quantifying the short-term temperature effect on lightsaturated photosynthesis on intertidal microphytobenthos. *Marine Ecology Progress Series,* **134**, 309–313.

Boussetta, S., Bassinot, F., Sabbatini, A., Caillon, N., Nouet, J., Kallel, N., Rebaubier, H., Klinkhammer, G., Labeyrie, L. (2011) Diagenetic Mg- rich calcite in Mediterranean sediments: Quantification and impact on foraminiferal Mg/Ca thermometry. *Marine Geology*, **280 (1–4),** 195–204.

Brasier, A.T., Andrews, J.E., Marca-Bell, A.D., Dennis, P.F. (2010) Depositional continuity of seasonally laminated tufas: Implications for $\delta^{18}O$ based palaeotemperatures. *Global and Planetary change*, **71 (3-4)**160 – 167.

Cacchio P, Ercole C, Cappuccio G, Lepidi A. (2003) Calcium carbonate precipitation by bacterial strains isolated from limestone cave and from a loamy soil. *Geomicrobiology Journal*, **20**, 85–98.

Cacchio P., Contento R., Ercole C., Cappuccio G., Martinez M. P. and Lepidi A. (2004) Involvement of microorganisms in the formation of carbonate speleothems in the Cervo Cave (L'Aquila—Italy). *Geomicrobiology Journal*, **21**, 497–509.

Chafetz, H., Rush, P.F. and Utech, N.M. (1991) Microenvironmental controls on mineralogy and habit of CaCO precipitates: an example from an active travertine system. *Sedimentology*, **38**, 107-126

Chave, K.E. (1954) Aspects of the biogeochemistry of magnesium: Calcareous marine organisms. *Journal of Geology*, **62**. 266–283.

Couradeau, E., Benzerara, K., Gérard, E., Estève, I., Moreira, D., Tavera, R. & López-García, P. 2013. Cyanobacterial calcification in modern microbialites at the submicrometer scale. *Biogeosciences*, **10**, 5255-5266.

Decho, AW. (2000) Microbial biofilms in intertidal systems: an overview. *Continental Shelf Research*, **20**, 1257–1273.

Decho, A.W. (2010) Overview of biopolymer-induced mineralization: What goes on in biofilms? *Ecological Engineering*, **36(2)**, 137-144.

Defew, E. C., Perkins, R. G., Paterson, D. M. (2004) The influence of light and temperature interactions on a natural estuarine microphytobenthic assemblage. *Biofilms*, **1**, 21–30.

Delaney, M.L., Be, A.W.H. and Boyle, E.A. (1985) Li, Sr, Mg and Na in foraminiferal calcite shells from laboratory culture, sediment traps, and sediment cores. *Geochimica Cosmochimica Acta*, **49**, 1327-1341.

Di Pippo, F.; Bohn, A.; Congestri, R.; De Philippis, R.; Albertano, P. Capsular polysaccharides of cultured phototrophic biofilms. *Biofouling*, **25**, 495-504

Dittrich, M., Muller, B., Mavrocordatos, D. and Wehrli, B., 2003. Induced calcite precipitation by cyanobacterium Synechococcus. Acta Hydrochimica Et Hydrobiologica,

31(2), 162-169.

Dittrich, M. and Sibler, S. (2010) Calcium carbonate precipitation by cyanobacterial polysaccharides. In: H.M. Pedley and M. Rogerson (Editors), *Speleothems and Tufas: Unravelling Physical and Biological controls*. Geological Society Special Publication. Geological Society of London, London, **336**, pp. 65-81.

Dupraz, C., Reid, P.R., Braissant, O., Decho, A.W. Norman, S.R. and Visscher, P.T. (2009). Processes of carbonate precipitation in modern microbial mats. *Earth Science Reviews,* **96(3)** 141-162.

Elderfield, H., Bertram, C.J. and Erez, J. (1996) Biomineralization model for the incorporation of trace elements into foraminiferal calcium carbonate, *Earth and Planetary Science Letters,* **142**, 409–423.

Fairchild, I.J. and Treble, P.C. (2009) Trace elements in speleothems as recorders of environmental change. *Quaternary Science Reviews*, **28**, 449–468

Garnett, E.R., Andrews, J.E., Preece, R.C., Dennis, P.F. (2004). Climatic change recorded by stable isotopes and trace elements in a British Holocene tufa. *Journal of Quaternary Science,* **19**, 251–262.

Geesey, G.G., Jang, L. (1989) Interactions between metal ions and capsular polymers. In: Beveridge, T.J., Doyle, R.J. (Eds.), *Metal ions and bacteria*. Wiley, New York, pp. 325–357.

Hancke, K. and Glud, R.N. (2004) Temperature effects on respiration and photosynthesis in three diatom-dominated benthic communities. *Aquatic Microbial Ecology,* **37**, 265-281.

Ihlenfeld C., Norman M., Gagan M., Drysdale R., Maas R. and Webb J. (2003) Climatic significance of seasonal trace element and stable isotope variations in a modern freshwater tufa. *Geochimica et Cosmochimica Acta,* **67**, 2341–2357

Kawaguchi, T. and Decho, A.W. (2002) Isolation and biochemical characterization of extracellular polymeric secretions (EPS) from modern soft marine stromatolites (Bahamas) and its inhibitory effect on $CaCO_3$ precipitation. *Biochemistry and Biotechnology,* **32**, 51–63.

Konhauser, K. (2007) *Introduction to Geomicrobiology*. Blackwell Publishing, Oxford.

Kısakürek, B., Eisenhauer, A., Böhm, F., Garbe-Schönberg, D. and Erez, J. (2008) Controls on shell Mg/Ca and Sr/Ca in cultured planktonic foraminiferan, Globigerinoides ruber (white). *Earth and Planetary Science Letters,* **273**, 260–269.

Lojen, S., Trkov, A., Ščančar, J., Vázquez-Navarro, Y.A. and Cukrov, N. (2009) Continuous 60-year stable isotopic and earth-alkali element records in a modern laminated tufa (Jaruga, river Krka, Croatia): Implications for climate reconstruction. *Chemical Geology*, **258**, 242–

598 250.
599
600 Lorens, R. B. (1981) Sr, Cd, Mn and Co distribution coefficients in calcite as a function of
601 calcite precipitation rate. *Geochimica et Cosmochimica Acta,* **45**, 553–561.
602
603 Martínez-Botí, M.A., Mortyn, P.G., Schmidt, D.N., Vance, D., Field, D.B. (2011) Mg/Ca in
604 foraminifera from plankton tows: Evaluation of proxy controls and comparison with core
605 tops. *Earth and Planetary Science Letters,* **307**, 113-125.
606
607 Mitsuguchi, T., Matsumoto, E., Abe, O., Uchida, T., Isdale, P.J., (1996) Mg/Ca thermometry
608 in coral skeletons. *Science,* **274**, 961–963.
609
610 Morse, J. W. and Bender, M. L. (1990) Partition coefficients in calcite: Examination of
611 factors influencing the validity of experimental results and their application to natural
612 systems. *Chemical Geol*ogy **82**, 265–277.
613
614 Morse, J.W. and Mackenzie, F.T. (1990) *Geochemistry of Sedimentary Carbonates*
615 *(Developments in Sedimentology).* Elsevier Science, London.
616
617 Mucci, A. (1987) Influence of temperature on the composition of magnesian calcite
618 overgrowths precipitated from seawater. *Geochimica et Cosmochimica Acta,* **51**, 1977-1984.
619
620 Nurnberg, D., Bijma, D. and Hemleben, C. (1996) .Assessing the reliability of magnesium in
621 foraminiferal calcite as a proxy for water mass temperatures, *Geochimica et Cosmochimica*
622 *Acta,* **60**, 803– 814.
623
624 Oomori T., Kaneshima H., and Maezato Y. (1987) Distribution coefficient of Mg^{2+} ions
625 between calcite and solution at 10–50°C. *Marine Chemistry* **20,** 327–336.
626
627 Pedley, H. M., Rogerson, M. and Middleton R. (2009) The growth and morphology of
628 freshwater calcite precipitates from in vitro mesocosm flume experiments. *Sedimentology,*
629 **56**, 511 – 527.
630
631 Pingitore, N.E., Eastmen, M.P., Sandidge, M., Oden, K., and Freiha, B. (1988) The
632 coprecipitation of manganese (II) with calcite: An experimental study. *Marine Chemistry,* **25**,
633 107–120.
634 Reynaud, S., Ferrier-Pages, C., Meibom, A., Mostefaoui, S., Mortlock, R., Fairbanks, R. and
635 Allemand, D. (2007) Light and temperature effects on Sr/Ca and Mg/Ca ratios in the
636 scleractinian coral Acropora sp. *Geochimica et Cosmochimica Acta,* **71**, 354 – 362.
637
638 Rimstidt J. D., Balog A., and Webb J. (1998) Distribution of trace elements between
639 carbonate minerals and aqueous solutions. *Geochimica et Cosmochimica Acta* **62,** 1851–
640 1863.
641
642 Rogerson, M., Pedley, H.M., Wadhawan, J.D. and Middleton, R. (2008) New insights into
643 biological influence on the geochemistry of freshwater carbonate deposits. *Geochimica et*
644 *Cosmochimica Acta,* **72**, 4976 – 4982.

Rogerson, M., Pedley, H.M., and Middleton, R. (2010) Microbial influence on macroenvironment chemical conditions in alkaline (tufa) streams: perspectives from *in vitro* experiments. In: H.M. Pedley and M. Rogerson (Editors), *Speleothems and Tufas: Unravelling Physical and Biological controls*. Geological Society Special Publication Geological Society of London, London, pp. 65-81.

Rosenthal, Y., Boyle, E.A. and Slowey, N. (1997) Environmental controls on the incorporation of Mg, Sr, F and Cd into benthic foraminifera shells from Little Bahama Bank: Prospects for thermocline paleoceanography. *Geochimica et Cosmochimica Acta,* **61**, 3633–3643, 1997.

Salleh, S. and McMinn, A. (2011) The effects of temperature on the photosynthetic parameters and recovery of two temperate benthic microalgae, amphora cf. coffeaeformis and cocconeis cf. sublittoralis (bacillariophyceae). *Journal of Phycology,* **47**, 1413-1424.

Saunders, P.V., Moulin, F.Y., Eiff, O., Rogerson, M. (In press) Biofilms. In: L.E Frostick, M.F. Johnson, R.E. Thomas, S.P. Rice and S.J.McLelland (Editors). *.A Users Guide to Ecohydraulic Experimentation*. IAHR book series, CRC Press, London.

Shirai K, Kusakabe M, Nakai S, Ishii T, Watanabe T, Hiyagon H, Sano Y. (2005) Deep-sea coral geochemistry: implication for the vital effect. *Chemical Geology*, **224**, 212–222

Shiraishi, F., Bissett, A., de Beer, D., Reimer, A., Arp, G. (2008a) Photosynthesis, respiration and exopolymer calcium-binding in biofilm calcification (Westerhöfer and Deinschwanger Creek, Germany). *Geomicrobiology Journal*, **25**, 83–94.

Shiraishi, F., Okumura, T., Takahashi, Y., Kano, A., (2010) Influence of microbial photosynthesis on tufa stromatolite formation and ambient water chemistry, SW Japan. *Geochimica et Cosmochimica Acta*, **74**, 5289–5304.

Tesoriero, A. and Pankow, J. (1996) Solid solution partitioning of Sr^{2+}, Ba^{2+}, and Cd^{2+} to calcite. *Geochimica et Cosmochimica Acta*, **60**, 1053–1063.

Wang, D.B., Wallace, A.F, De Yoreo, J.J., Dove, P.M. (2009) Carboxylated molecules regulate magnesium content of amorphous calcium carbonates during calcification. *Proceedings of National Academy of Sciences U.S.A.,* **106**, 21511–21516

Watermanm F., Hillebrand, H., Gerdes, G., Krumbein, W.E., Sommer, U. (1999). Competition between benthic cyanobacteria and diatoms as influenced by different grain sizes and temperatures. *Marine Ecology Progress Series,* **187**, 77-87.

Wei, G., Sun, M., Li, X., Nie, B., (2000) Mg/Ca, Sr/Ca and U/Ca ratios of a porites coral from Sanya Bay, Hainan Island, South China sea and their relationships to sea surface temperature. *Palaeogeography Palaeoclimatology Palaeoecology*, **162**, 59–74.

691 Wolfaardt, G.M., Lawrence, J.R., Robarts, R.D., Caldwell, D.E. (1998) In situ
692 characterization of biofilm exopolymers involved in the accumulation of chlorinated
693 organics. *Microbiolial Ecology,* **35**, 213–223.
694
695 Yoshimura, T., Tanimizu, M., Inoue, M., Suzuki, A., Iwasahi, N., Kawahata, H. (2011) Mg
696 isotope fractionation in biogenic carbonates of deep-sea coral, benthic foraminifera, and
697 hermatypic coral. *Analytical and bioanalytical chemistry*, **401(9)**, 2755 – 2769.
698
699 Yu, K.F., Zhao, J.X., Wei, G.J., Cheng, X.R., Chen, T.G., Felis, T., Wang, P.X., Liu, T.S.
700 (2006) $\delta^{18}O$, Sr/Ca and Mg/Ca records of Porites lutea corals from Leizhou Peninsula,
701 northern South China Sea, and their applicability as palaeoclimatic indicators.
702 *Palaeogeography, Palaeoclimatology, Palaeoecloogy,*, **218**, 57–73.
703
704 Zhang, Y. and Dawe, R.A. (2000) Influence of Mg^{2+} on the kinetics of calcite precipitation
705 and calcite crystal morphology. *Chemical Geology,* **163**, 129-138.
706

707 Captions

708
709 Fig. 1. Schematic visualisation of the addition of the agitated 659 flask experiment to the microcosm
710 design. Arrows indicate direction of water flow.
711
712 Fig. 2. $(Mg/Ca)_{calcite}$ ratios as a function of temperature: (a) Microcosms; (b) BFL; (c) BFD; (d)
713 Combined data. Error bars represent 1 σ.
714
715 Fig. 3. Precipitation rate versus temperature. (a) Microcosms; (b) BFL; c) BFD; (d) Combined data.
716
717 Fig. 4. $(Mg/Ca)_{calcite}$ as a function of precipitation rate (a) Microcosms; (b) BFL; (c) BFD; (d) Combined
718 data.
719
720 Fig. 5. (a) Mean precipitation rates of all replicates from the microcosm, BFL and BFD experiments as
721 a function of temperature. (b) Mean precipitation rate as a function of temperature excluding the 20
722 °C data.
723
724 Fig. 6. Distribution coefficients as a function of precipitation rate from the microcosm and agitated
725 flask experiments combined.
726
727 Fig. 7. Schematic representation of unidentate and bidentate bonding of cations on anionic groups
728 of EPS molecules (represented by the two wavy lines). Nucleation sites are created on unidentate
729 bonded Ca_{2+}673 . The large arrows represent the continuous diffusion of ionic species into and out of
730 the microenvironment of the EPS molecules.
731
732 Table 1. Empirical and equilibrium distribution coefficients for selected divalent cations along with
733 ionic radii. The ionic radii are in six-fold coordination from Shannon and Prewitt, 1969. For reference
734 the ionic radii of Ca^{2+} is 1.00 (Table adapted from Rimstidt *et al.*, 1998).
735
736 Table 2. Binding constants for multicarboxylic acids. The Binding constant *K* is for the generalised
737 association reaction M+L ⇄ ML, with M representing the metal cation and L the ligand (adapted
738 from Wang *et al.*, 2009).

BENZERARA, K., MENGUY, N., LOPEZ-GARCIA, P., YOON, T.-H., KAZMIERCZAK, J., TYLISZCZAK, T., GUYOT, F. & BROWN, G. E., JR. 2006. Nanoscale detection of organic signatures in carbonate microbialites. *Proceedings of the National Academy of Sciences* 103**,** 9440-9445.

COURADEAU, E., BENZERARA, K., GÉRARD, E., ESTÈVE, I., MOREIRA, D., TAVERA, R. & LÓPEZ-GARCÍA, P. 2013. Cyanobacterial calcification in modern microbialites at the submicrometer scale. *Biogeosciences,* 10**,** 5255-5266.

DECHO, A. W. 2010. Overview of biopolymer-induced mineralization: What goes on in biofilms? *Ecological Engineering,* 36**,** 137-144.

PEDLEY, H. M., ROGERSON, M. & MIDDLETON, R. 2009. The growth and morphology of freshwater calcite precipitates from in Vitro Mesocosm flume experiments; the case for biomediation. *Sedimentology,* 56, **,** 511-527.

ROGERSON, M., PEDLEY, H. M., WADHAWAN, J. D. & MIDDLETON, R. 2008. New Insights into Biological Influence on the Geochemistry of Freshwater Carbonate Deposits. *Geochimica et Cosmochimica Acta,* 72**,** 4976-4987.

Table 1. Empirical and equilibrium distribution coefficients for selected divalent cations along with ionic radii. The ionic radii are in six-fold coordination from Shannon and Prewitt, 1969. For reference the ionic radii of Ca^{2+} is 1.00 (Table adapted from Rimstidt *et al*., 1998).

Cation	Ionic radius	K_{exp}	K_{eq}
Ba^{2+}	1.36	0.020	1.95×10^{-2}
Cd^{2+}	0.95	188	6.92×10^{3}
Co^{2+}	0.65	10.9	4.68×10^{1}
Cu^{2+}	0.73	80.2	1.55×10^{3}
Fe^{2+}	0.61	27.7	2.40×10^{2}
Mg^{2+}	0.72	0.022	8.71×10^{-4}
Mn^{2+}	0.67	20.5	1.41×10^{2}
Pb^{2+}	1.18	17.2	2.63×10^{3}
Ra^{2+}	1.44	0.020	1.91×10^{-3}
Sr^{2+}	1.16	0.073	1.82×10^{-1}

Table 2. Mean precipitation rates from lowest to highest as related to experimental conditions.

Experiment type	Temperature (°C)	Precipitation rate ($\mu mol\ cm^{-2}\ hr^{-1}$)
Microcosm	12	0.027
Microcosm	14	0.047
Microcosm	16	0.007
Microcosm	18	0.065
Microcosm	12	0.027
BFL	12	0.012
BFL	14	0.107
BFL	16	0.113
BFL	18	0.023
BFL	20	0.177
BFD	12	0.006
BFD	14	0.056
BFD	16	0.034
BFD	18	0.036
BFD	20	0.116

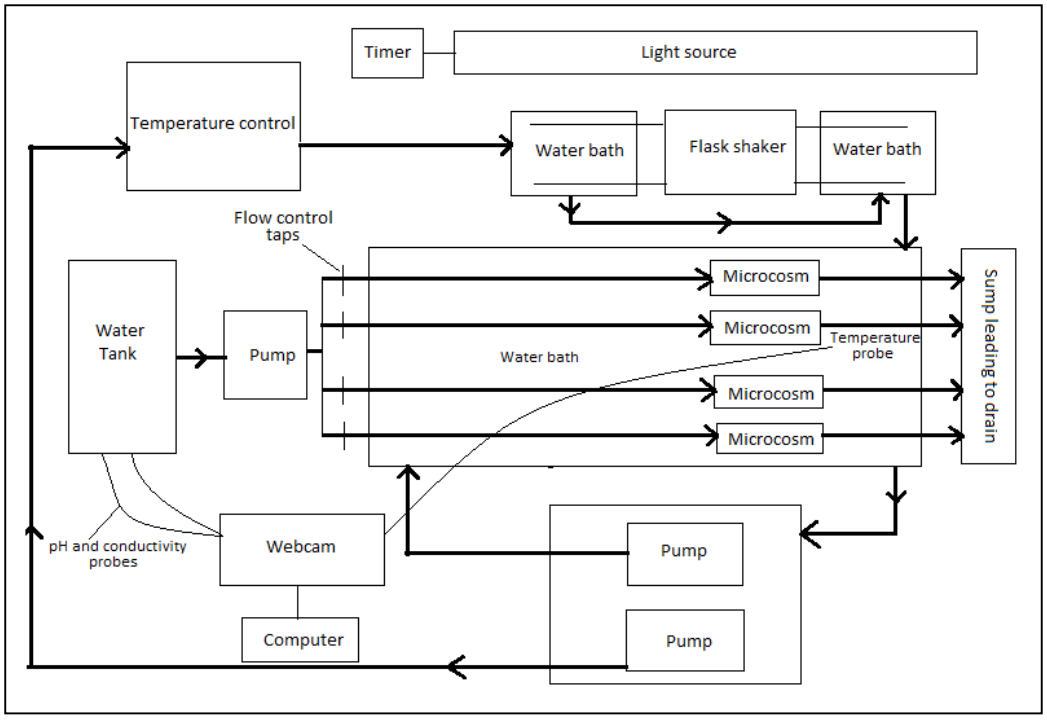

Figure 1. Schematic visualisation of the addition of the agitated flask experiment to the microcosm design. Arrows indicate direction of water flow.

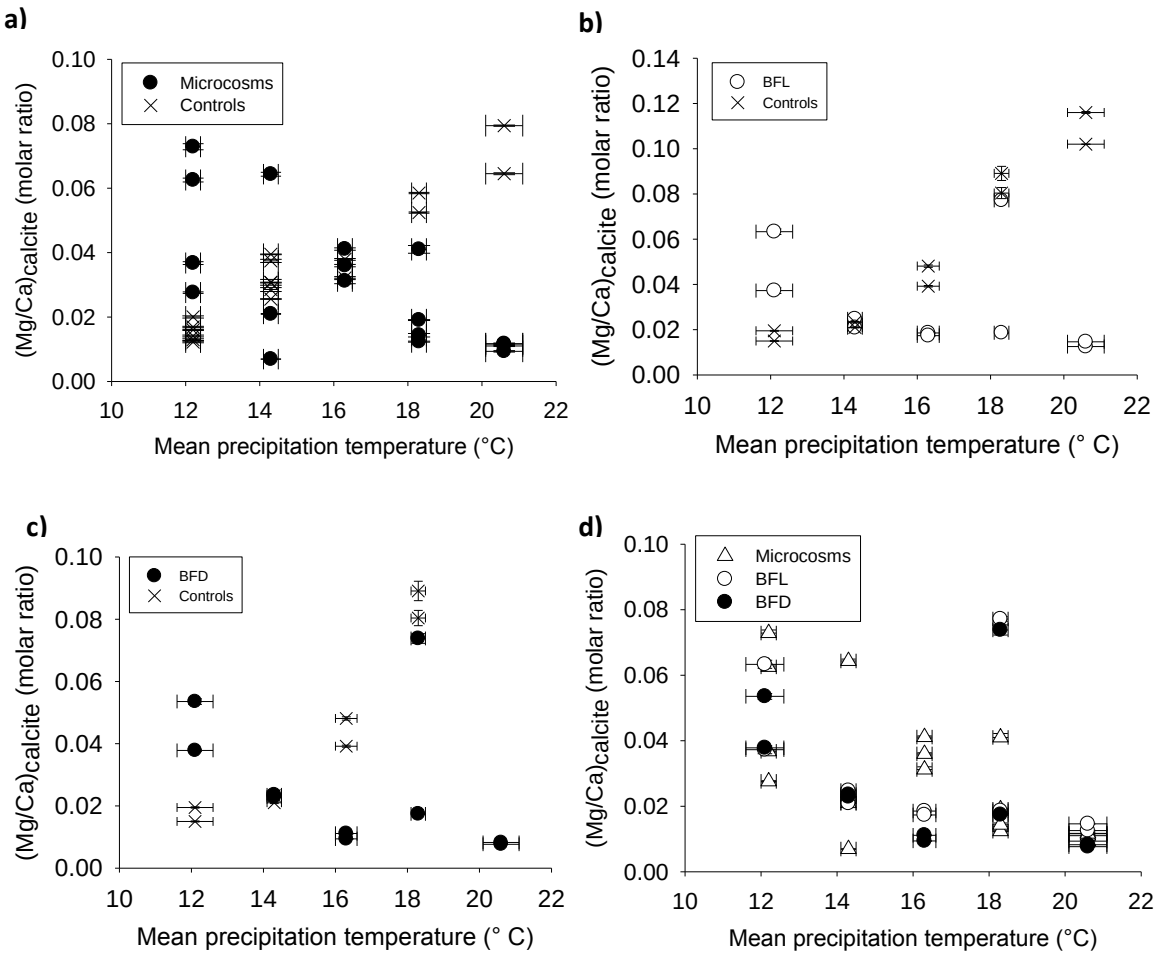

Figure 2. $(Mg/Ca)_{calcite}$ ratios as a function of temperature: (a) Microcosms; (b) BFL; (c) BFD; (d) Combined data. Error bars represent 1 σ.

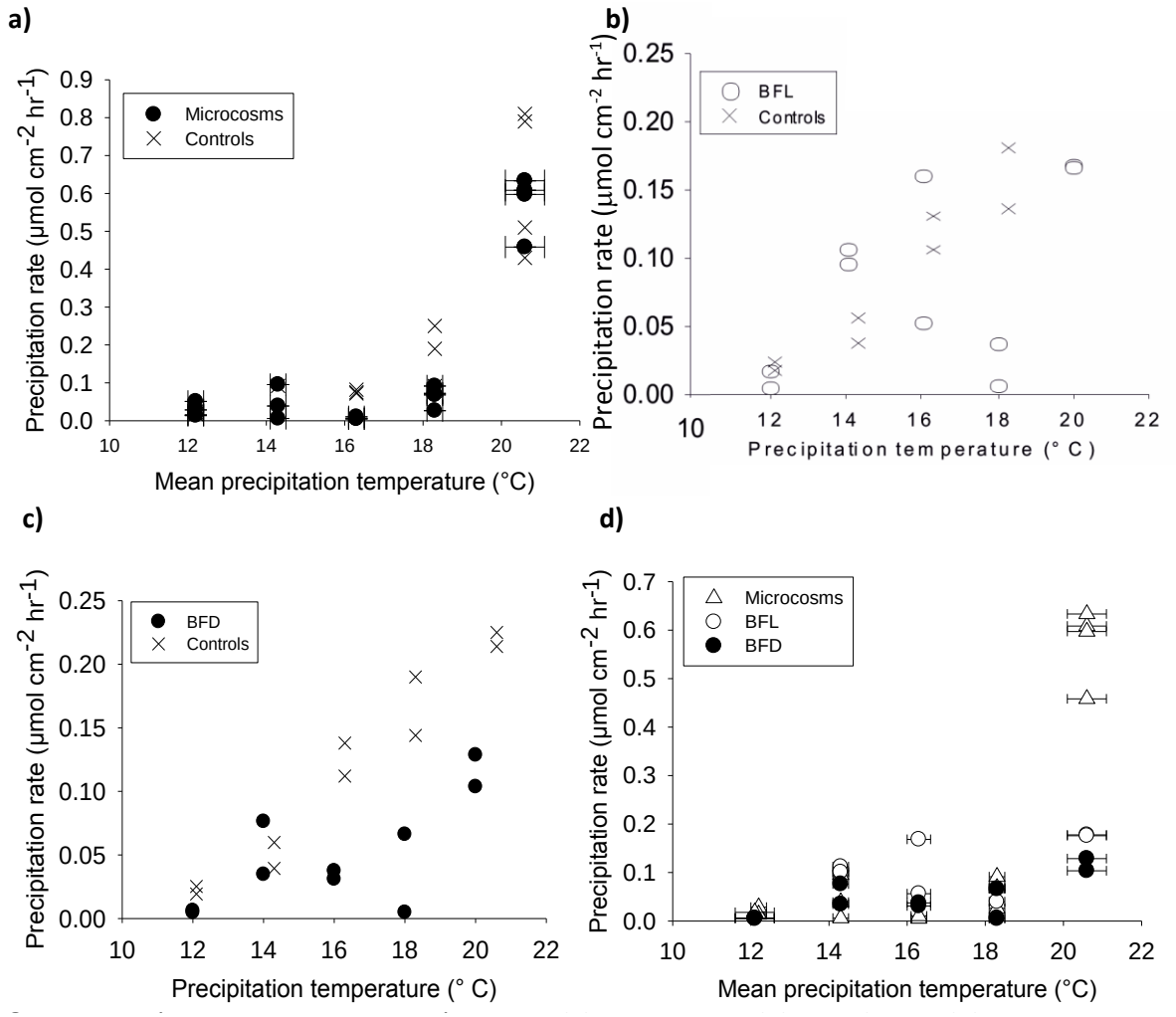

Fig. 3. Precipitation rate versus temperature. (a) Microcosms; (b) BFL; c) BFD; (d) Combined data.

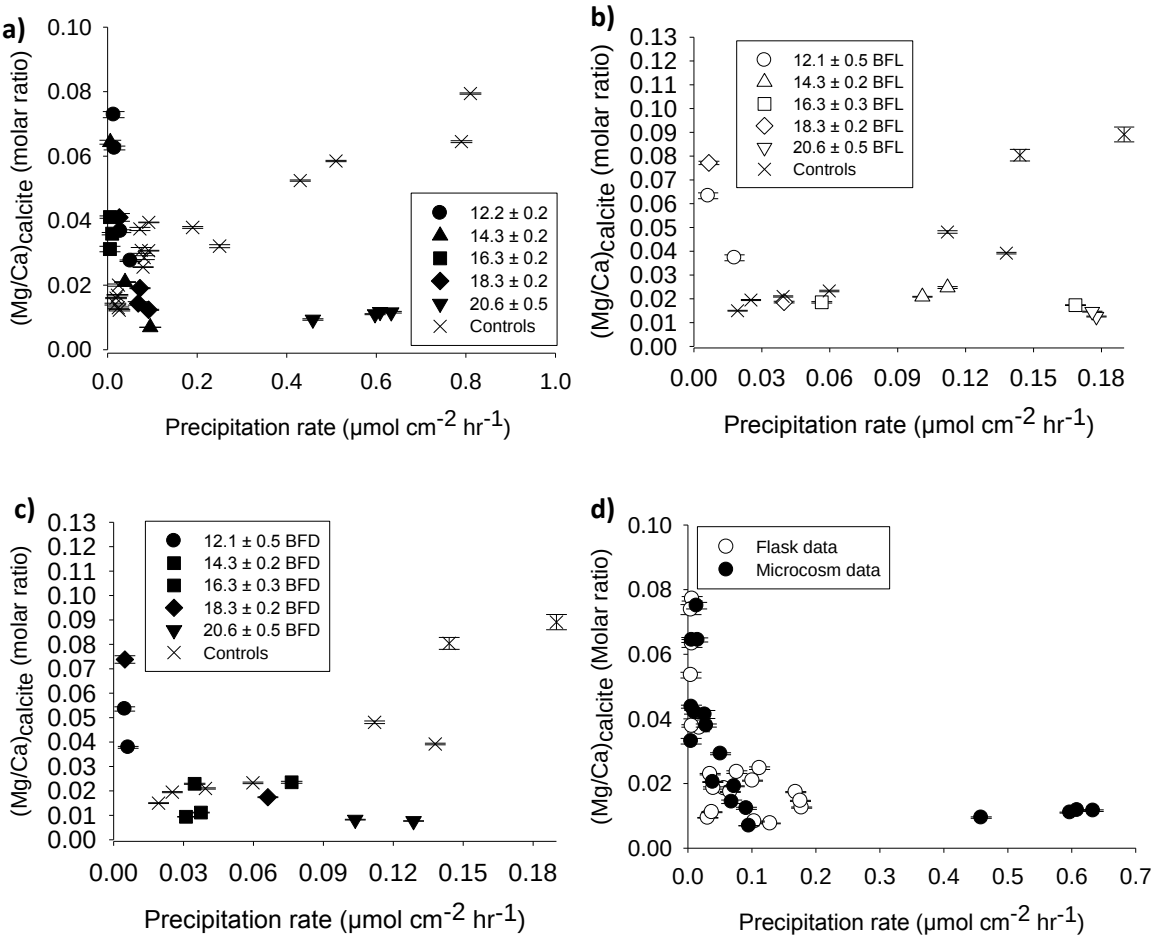

Figure 4. $(Mg/Ca)_{calcite}$ as a function of precipitation rate (a) Microcosms; (b) BFL; (c) BFD; (d) Combined data.

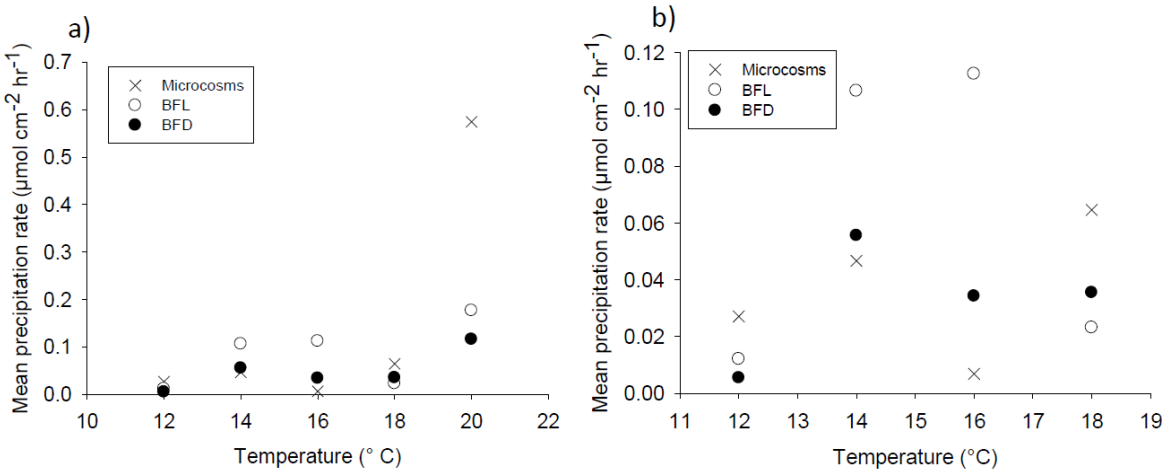

Fig. 5. (a) Mean precipitation rates of all replicates from the microcosm, BFL and BFD experiments as a function of temperature. (b) Mean precipitation rate as a function of temperature excluding the 20 °C data.

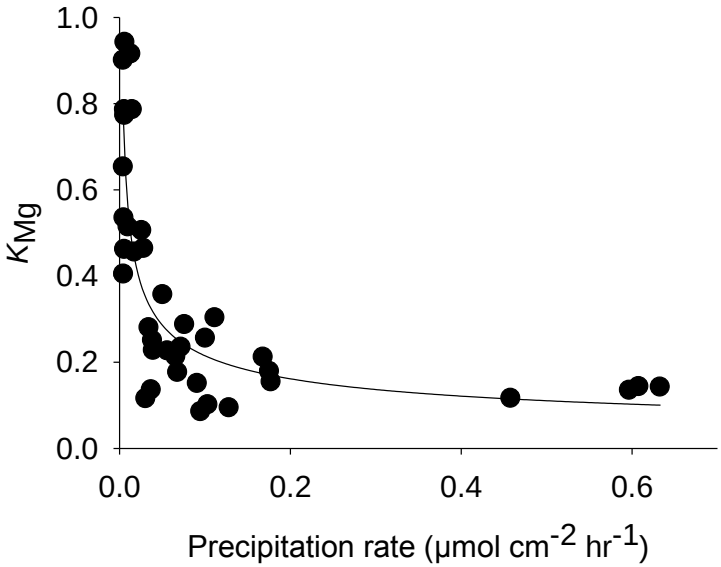

Figure 6. Distribution coefficients as a function of precipitation rate from the microcosm and agitated flask experiments combined.

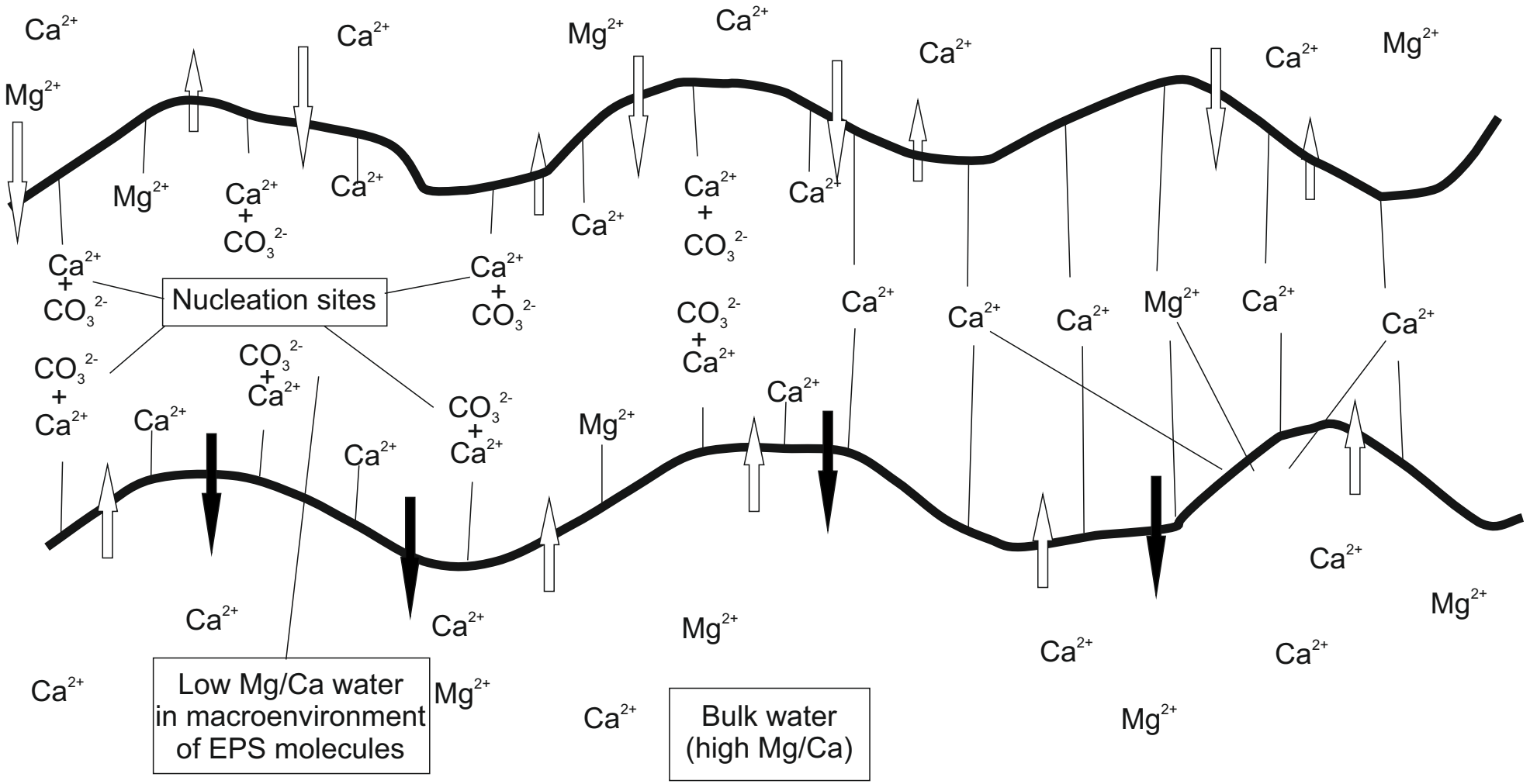

Fig. 7. Schematic representation of unidentate and bidentate bonding of cations on anionic groups of EPS molecules (represented by the two wavy lines). Nucleation sites are created on unidentate bonded Ca^{2+} . The large arrows represent the continuous diffusion of ionic species into and out of the microenvironment of the EPS molecules.